4. Results

Part I- *dre-1*

4.1. Screen for *daf-12* redundant functions

In response to the environment, the nuclear hormone receptor *daf-12* chooses between L3 options of reproductive growth and dauer formation. Null mutants of *daf-12* are fully dauer defective, revealing an essential role in dauer formation. By contrast, null mutants have impenetrant defects in L3 reproductive programs, including delayed heterochronic phenotypes in gonadal and extragonadal tissues, suggesting that redundant functions may act together with *daf-12* to specify reproductive growth.

To identify *daf-12 re*dundant (*dre*) functions we performed a screen using *daf-12* null as a genetic background to look for enhancement of *daf-12* heterochrony. *daf-12(rh61rh411)* hermaphrodites were mutagenized by EMS, and 127000 genomes were screened for a synergistic enhancement of heterochronic gonadal migration defects (SynMig) (Figure 4.1.). The screen yielded 9 Mig mutants: *dh99, dh172, dh184, dh190, dh278, dh279, dh280, dh284* and *dh292*. Complementation tests revealed that two different loci, termed *dre-1* and *dre-2,* were identified. Eight mutants belonged to *dre-1*, while one (*dh184*) belonged to *dre-2*. We focused first on *dre-1* (this chapter) and secondly on *dre-2* (next chapter).

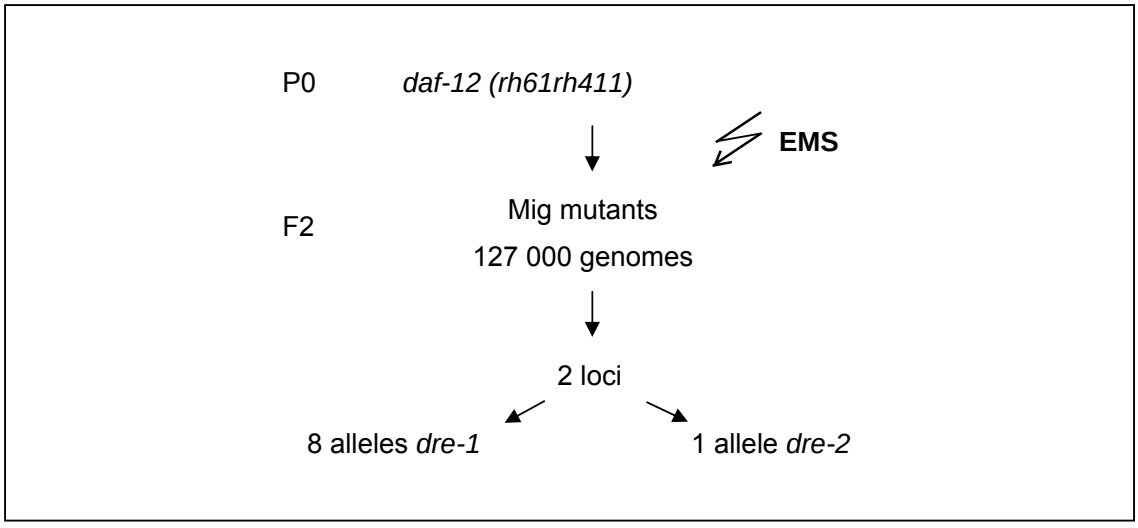

Figure 4.1. Screen for *daf-12* redundant functions.
Scheme of an EMS F2 mutant screen for the synergistic enhancement of the gonadal Mig phenotype of *daf-12* null mutant *rh61rh411.*

4.2. *dre-1* influences gonadal heterochrony

Gonad outgrowth is led by the Distal Tip Cells (DTC), which change motility and direction to guide the final shape of the gonad arms. During larval development the DTC undergo stage-specific migratory events termed S2, S3, S4, SA, which roughly start at the midpoint between larval molts (Antebi et al., 1998). Beginning at the early-L2 stage, wild type DTC start to migrate longitudinally towards head and tail, expressing a short S2 program. By mid-L2 they start their S3 programs, in which migration direction is maintained. By mid-L3 they begin their S4 programs, where the DTC halt, turn dorsally across the lateral hypodermis, reorient and then migrate centripetally back towards midbody, a process termed reflexion. By mid-L4, the DTC begin the adult specific program SA, where the DTC slow down, and continue migration towards mid-body and then finally halt (Figure 4.2.A).

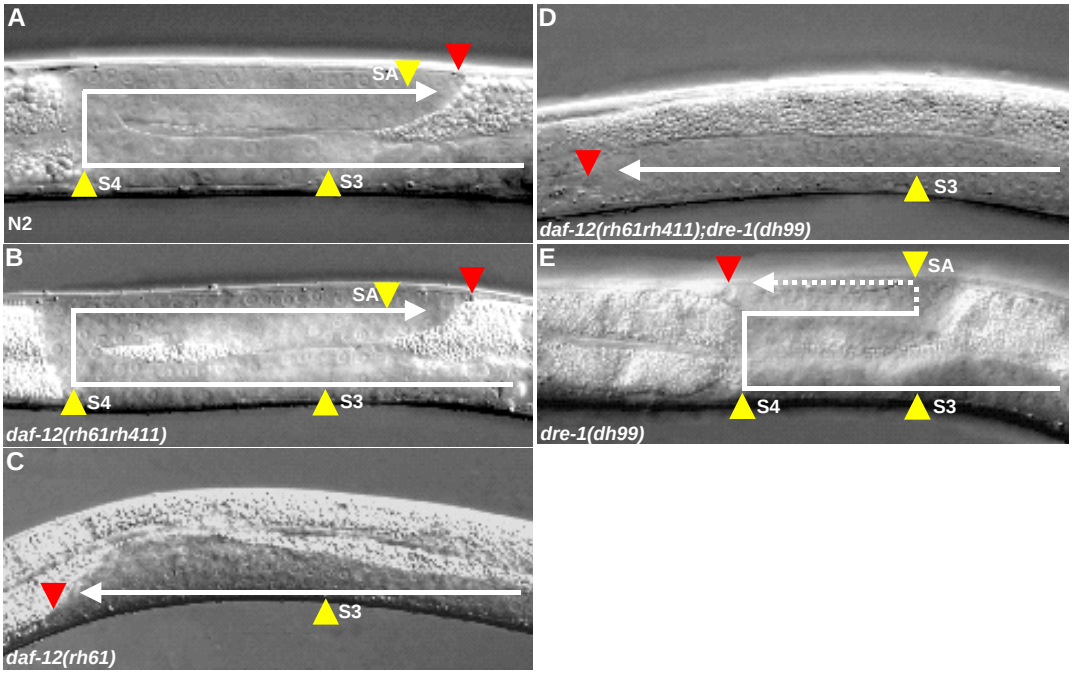

Figure 4.2. Gonadal heterochrony.
Gonadal Mig phenotypes of *daf-12* and *dre-1* single and double mutants. (A) wild type N2 (B) *daf-12* null mutant *rh61rh411* (C) *daf-12* gain-of-function mutant *rh61* (D) *daf-12(rh61rh411);dre-1(dh99)* double mutant (E) *dre-1(dh99)* single mutant. White lines show migration of the gonad. Red arrowhead indicates distal tip cell; yellow arrowheads the starts of appropriate stage-specific gonadal migration programs (S3, S4, SA).

daf-12 null allele *rh61rh411* displays no or a very mild gonad migration defect (Figure 4.2.B), in which the DTC occasionally fail to turn back towards midbody (Antebi et al., 1998). However, in a number of *daf-12* ligand binding mutants, such as *rh61,* gonadal migration is strongly delayed. Gonadal arms are completely unreflexed and instead continue to migrate towards head and tail on the ventral body wall (Figure 4.2.C). Failure to turn is interpreted as

an inappropriate repetition or arrest of S2/S3 pathfinding programs. At the molecular level, it is thought that unliganded *daf-12* acts as a gain-of function that constitutively represses expression of later programs. Null alleles have weaker phenotypes presumably because other loci are also involved in activating gonadal outgrowth.

dre-1;*daf-12* null double mutants displayed a severely delayed gonadal migration defect with high penetrance (Figure 4.2.D, Table 4.1.). This SynMig strongly resembled that seen in *daf-12(rh61)*, in which reflexion fails or does not occur on schedule. Alone, *dre-1* single mutants displayed only weak impenetrant gonadal cell migration defects, including extra turns of gonadal arms (Figure 4.2.E, Table 4.1.). In particular, after completing reflexion and reorienting towards midbody, the DTC occasionally reversed direction and began migration back towards head and tail. This could be interpreted as a failure to execute the SA program or a reiteration of earlier programs. The synergistic Mig phenotypes suggest that somehow *daf-12* and *dre-1* act in a parallel pathway to co-activate S4 programs in the gonad.

4.3. dre-*1* is an allele non-specific Mig enhancer of *daf-12*

The *daf-12* null allele *rh61rh411* is an intragenic non-Mig revertant of *daf-12(rh61).* It carries two stop codons, one in the DNA binding domain and another in the ligand binding domain. It belongs to *daf-12* class 3 alleles, which generally correspond to the null phenotype, and predominately harbor mutations in the DNA binding domain. We asked whether the interaction with *dre-1* was allele specific. Therefore, we crossed *daf-12(m421)* and *daf-12(sa156)* to *dre-1(dh99)*. Both *daf-12* alleles have missense lesions within conserved residues of the DNA binding domain and display impenetrant heterochrony (Antebi et al., 2000). By contrast, all double mutants displayed the Mig phenotype indicating that *dre-1* interacts with *daf-12* in an allele non-specific manner. Accordingly, *daf-12* RNAi gave the same phenotype (Table 4.3). Finally, another allele of *dre-1(dh190)* gave the Mig phenotype on *daf-12* RNAi (Table 4.3.), revealing that the interaction between *dre-1* and *daf-12* is allele non-specific.

4.4. *dre-1* regulates the larval to adult switch in seam cells

Seam cells are lateral epidermal cells that undergo stage specific lineage patterns termed S1-S4 and SA, which appear coordinated with the larval molt cycle. At early larval stages they typically undergo a stem cell division, in which the anterior daughter fuses with the hypodermal syncitium while the posterior cell continues division in the subsequent stage. Stage-specific ornamentation of this pattern occurs in S2 programs, where equational division precedes stem cell division, increasing the number of seams from 10 to 16.

However, the most dramatic stage specific difference is the SA program, or larval to adult switch. At the L4 molt, seam cells exit the cell cycle, fuse and terminally differentiate. One conspicuous marker of differentiation is adult alae, a ridged cuticular structure synthesized by the seam syncitium. Precocious mutants omit stage-specific programs resulting in a premature terminal differentiation of the hypodermis. Conversely, delayed mutants reiterate programs of earlier larval stages resulting in delayed terminal differentiation of the hypodermis.

In *dre-1(dh99)* animals seam cell development appeared essentially normal until L3. However, at the L3 molt, *dre-1* expressed adult programs (SA) one stage early: seam cells fused and adult alae were synthesized (Figure 4.3.D, E). Thus, *dre-1* causes precocious seam development. Precocious adult alae were seen with low penetrance. Only 15% of the *dre-1* animals exhibited the phenotype (Table 4.4.). Of these, 33% of the seam cells produced precocious alae (Table 4.5.). In addition, the precocious alae were often indistinct and difficult to detect compared to adult alae of wild type animals (Figure 4.3.C, D). Therefore, we used seam cell fusion as an additional marker for precocious maturation. Cell fusion was monitored employing the transgene *ajm-1::gfp* that marks seam cell junctions. Wild type expressing *ajm-1::gfp* displayed unfused seam cells at the L3 molt, and instead divided (S4 program) (Figure 4.3.B, Table 4.4.). In contrast, 85% of *dre-1* animals carrying the *ajm-1::gfp* marker exhibited precocious fusion of seam cells at the L3 molt (Figure 4.3.E, Table 4.4.). In each animal, about half of cells (52%) were fused (Table 4.5.).

Surprisingly, *dre-1* also displayed gaps in the adult alae at the L4 molt. This phenotype is typically seen in delayed heterochronic mutants, in which seam cells continue to divide instead of expressing SA programs. However, closer inspection of *dre-1* mutants revealed that gapped cells had also ceased division, and thus may have a different problem related to seam maturation (Figure 4.3.F, Table 4.1.). About half of the *dre-1(dh99)* animals display the alae gap phenotype and of these 20% of seam cells were affected (Table 4.4.). To find out whether the specification of L4 and adult seam cell fates were lineally correlated, we examined the seams of individual animals at the L3 and L4 molts. At the L3 molt, seam cells with normal S4 program (cell division), either expressed SA programs appropriately at the next stage giving rise to adult alae, or not, giving rise to alae gaps. Therefore, no correlation was apparent. Since it was difficult to determine which cells were undergoing precocious differentiation at the L3 molt, we were not able to ask what happens to these cells in the next stage. In this regard, lineage analysis of *dre-1* seam cell phenotypes in the *ajm-1::gfp* background could greatly clarify programming defects.

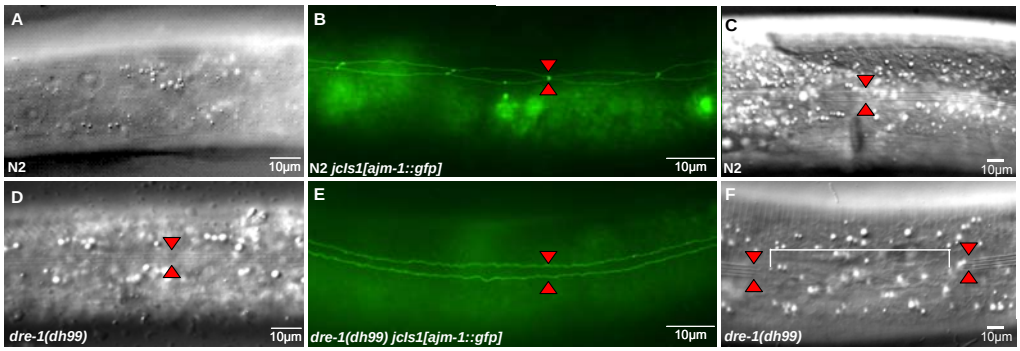

Figure 4.3. Heterochronic seam cell phenotype.
(A) to (C) wild type N2. (A) L3 molt without adult alae. (B) L3 molt, N2 with *ajm-1::gfp* fusion depicting dividing, unfused seam cells. (C) Young adult with continuous adult alae.
(D) to (F) *dre-1(dh99).* (D) L3 molt with precocious adult alae. (E) L3 molt, *dre-1(dh99)* with *ajm-1::gfp* fusion depicting precociously fused seam cells. (F) Young adult with gaps in the adult alae. Red arrowheads indicate unfused seam cells (B), adult alae (C), precocious adult alae (D), fused seam cells (E). In (F) red arrowheads together with the white bracket indicate a gap in the adult alae.

Late stage mutant phenotypes of *daf-12* and other heterochronic genes can be suppressed when animals develop through dauer, presumably because of temporal reprogramming (Antebi et al., 1998; Liu et al., 1995). Similarly, the *dre-1* alae gap phenotype was suppressed in post dauer animals (Table 4.4.).

4.5. Phenotypic classes

dre-1 alleles could be grouped into two classes. Class 1 alleles displayed penetrant alae gap phenotypes, whereas class 2 alleles had no or very impenetrant defects. Both classes of *dre-1* alleles exhibited weak Mig phenotypes (see above), with the penetrance varying from 2 to 24 % and were indistinguishable for their SynMig gonadal phenotypes.

Table 4.1. *dre-1* phenotypic classes

Class	Genotype *dre-1* alleles	% of animals with Mig phenotype	% of animals with adult alae gap phenotype @L4m
N2		0	0
Class 1	*dh99*	10[a]	45
	dh190	24[a]	42
	dh292	nd	nd
Class 2	*dh278*	nd	nd
	dh284	nd	nd
	dh172	24[a]	8
	dh280	nd	nd
	dh279	2[a]	0
Class 1	*dh99*	100[b]	56
in *daf-12(rh61rh411)*	*dh190*	100[b]	24
background	*dh292*	100[b]	28
Class 2	*dh278*	100[b]	4
in *daf-12(rh61rh411)*	*dh284*	100[b]	8
background	*dh172*	98[b]	8
	dh280	100[b]	0
	dh279	100[b]	0

nd: not determined; n=25 adult animals; [a]Mig phenotype of class 1 (see Figure 4.7.); [b]Mig phenotype of class 1 (see Figure 4.7.); class 1 and 2 single mutants with missing numbers for delayed adult seam phenotype have been grouped based on their adult seam phenotypes in the *daf-12(rh61rh411)* background.

4.6. *dre-1* encodes an evolutionary conserved F-box protein

4.6.1. Mapping *dre-1*

Using snip markers we mapped *dre-1* to the center of chromosome V (Figure 4.4.A). 3-factor mapping confirmed the position between *unc-46* (-2.36 map units) and *unc-42* (2.17 map units). Deficiency mapping suggested that *dre-1* was located between (-0.47) and (-0.17). Further snip mapping narrowed the region down to YAC Y40G12 (for detailed mapping data see material and methods 3.2). Transgenic animals harboring an extrachromosomal array of

Y40G12 rescued the *dre-1* alae gap and SynMig phenotypes. All *dre-1(dh99) dhEx231* and *dre-1(dh99)dhEx185* animals had normal seam cell development (n=50). However, only two of twenty lines gave rescue. In addition, rescue experiments microinjecting cosmids spanning the Y40G12 region were unsuccessful. Sequence analysis of ORFs (predicted by www.wormbase.org, WormBase Release115) in the Y40G12 region identified *dre-1* as K04A8.6.

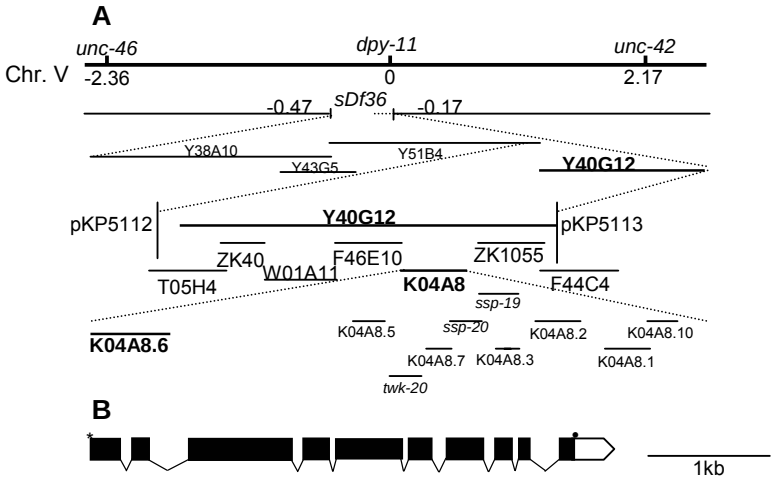

Figure 4.4. *dre-1* encodes an evolutionary conserved F-box protein.
(A) Genomic organization. *dre-1* maps to linkage group V on the right side of *dpy-11*. Deletion, YACs, cosmids and snipSNPs (pKPs) are indicated below the genetic map.
(B) *dre-1* structure. Asterisks indicates the start codon, black filled circle the stop codon. Exons are indicated by dark boxes, 3'UTR by a white box.

4.6.2. *dre-1* structure

The 2811 bp *dre-1* ORF encoded a protein of 937 aa. The genomic region spanned 4434 bp, comprising of 10 exons and a 3'UTR of 336 bp (Figure 4.4.B). Sequence analysis of *dre-1* EST clones (provided by Y. Kohara) confirmed predicted intron/exon borders (yk1132 and yk87b4), but also revealed a splice variant that contained an additional intron between exon 3 and four 4 (YK1132). When translated the additional intron generated a stop codon (TGA) at its first codon, resulting in a truncation of the protein at 474 aa and elimination of important protein domains. Whether this splice variant is functional remains to be determined.

4.6.3. *dre-1* encodes an evolutionary conserved F-box protein

Blast analysis revealed that *dre-1* contains several conserved protein family domains (Figure 4.5.), including an N-terminal F-box domain, central PbH1 motifs embedded within three CASH domains, a NosD domain, and a C-terminal Zinc finger similar to that found in N-recognin (ZnF_UBR1). Notably, the F-box motive is implicated in interactions with proteins such as yeast Skp-1 and homologs. Skp-1 and F-box proteins are known components of the

SCF (Skp-1, Cullin and F-box) E3 ubiquitin ligase complex that is involved in protein degradation. The PbH1 domains are Parallel beta-helix repeats first seen in pectate lyases that bind β-galactose containing polymers (Jenkins et al., 1998). CASH domains are found in many carbohydrate-binding proteins and sugar hydrolases that contain internal repeats of glycines and hydrophobic residues. These correspond to repeats in the righthanded β-helix structure of the pectate lyase superfamily (Ciccarelli et al., 2002). The NosD domain is the copper binding component of N_2O reductase complexes of bacteria. It overlaps with the CASH and PbH1 domains. The ZnF_UBR1 is a zinc finger domain of N-recognin, an E3 ligase that is involved in substrate recognition of N-end rule substrates in yeast UBR1. The N-end rule relates the *in vivo* half-life of a protein to its N-terminal residue. Two protein motives found in DRE-1, the F-box and the Zinc finger in N-recognin imply *dre-1* could function in protein degradation. In addition, DRE-1 was predicted to be localized to the nucleus using protein analyze programs (PSORT: 7 nuclear localization signals, 69,6% nuclear prediction (Figure 4.6.)).

4.6.4. DRE-1 orthologs

Database searches revealed that DRE-1 is an ancient protein with clear orthologs in closely related *C. briggsae* (CBG18961) (E-value: 0), as well as *Drosophila melanogaster* (CG9461) (E-value: 0), *Rattus norvegicus* (Q7TSL3) (E-value: 0), and humans (VIT-1) (E-value: 0) (Figure 4.5).

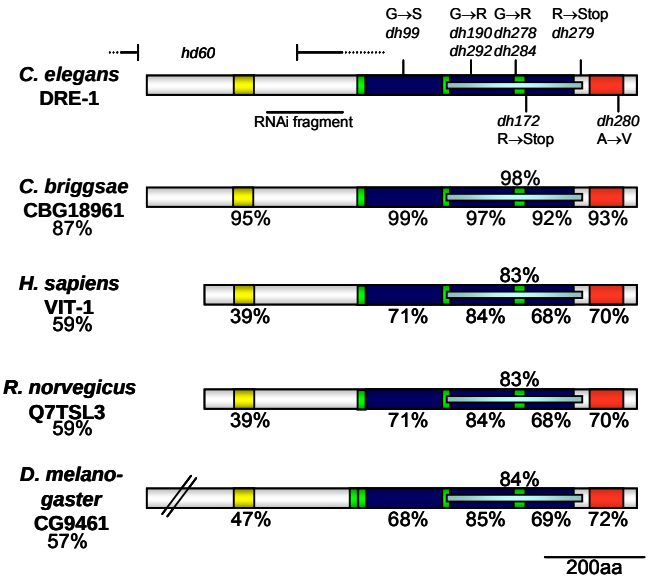

Figure 4.5. Schematic diagram of DRE-1 and its orthologs.
Protein domains: F-box, yellow; CASH, blue; PbH1, green; NosD, light blue; Zinc finger, red. Percentage identities are given relative to DRE-1. *dre-1* mutations (*dh* alleles), deletion (*hd60*) and RNAi fragment are indicated above the diagram.

These orthologs were highly homologous and had the same domain architecture as DRE-1 (Figure 4.6.). Additionally, they were similar in size, except *D. melanogaster* CG9461, which contained an extended N-terminus (Figure 4.5.).

The closest *C. elegans* relative was BE0003N10.3 (CE28429) (E-value: e -123), which was of similar structure, but lacked the F-box domain. Moreover, RNAi of this homologue had no observable phenotype (data not shown). DRE-1 protein domains were also very conserved among species. The homology of NosD was highest, followed by CASH and the zinc finger domains (Figure 4.5.). The least conserved domain was the F-box, though identities were still significant ranging from 39-95%. While DRE-1 orthologs in *C. briggsae*, *D. melanogster*, and *C. elegans* BE0003N10.3 are uncharacterized, human VIT-1 (Vitiligo associated protein 1) is involved in the multigenic skin disorder vitiligo (Le Poole et al., 2001). In vitiligo lesions, melanocytes, the pigment producing cells of the skin, are eliminated. VIT comes in three isoforms (843, 258, 157 aa) and is expressed at very low levels in different skin cell types as melanocytes, keratinocytes and fibroblasts. It is downregulated in vitiligo, but no function has been assigned. Thus, *dre-1* is the first gene within this conserved protein family with an ascribed function.

Figure 4.6. Multiple sequence alignment of DRE-1 with its orthologs.
Identical amino acids are shaded in black, chemically similar residues in grey. Protein motifs and mutations are indicated. F-box is indicated by a yellow bar, CASH domains in blue, NosD in light blue, Zinc finger in red. 18 PbH1 domains are found between position 405 to 818. For simplicity only 3 PbH1 domains that locate between CASH domains are indicated. Amino acid changes caused by mutations are indicated by a red circle above the alignment. Three of seven nuclear localization signals are indicated by an orange bar (Other nuclear localization signals are PYSLRKR at position 77, RKRR at position 81, KRRP at position 82 and PTMKKFK at position 108). Abbreviations used: C.e.: *C. elegans*; C.b. *C. briggsae*; R.n.: *R. norvegicus*; H.s.: *H. sapiens*; D.m.: *D. melanogaster.*

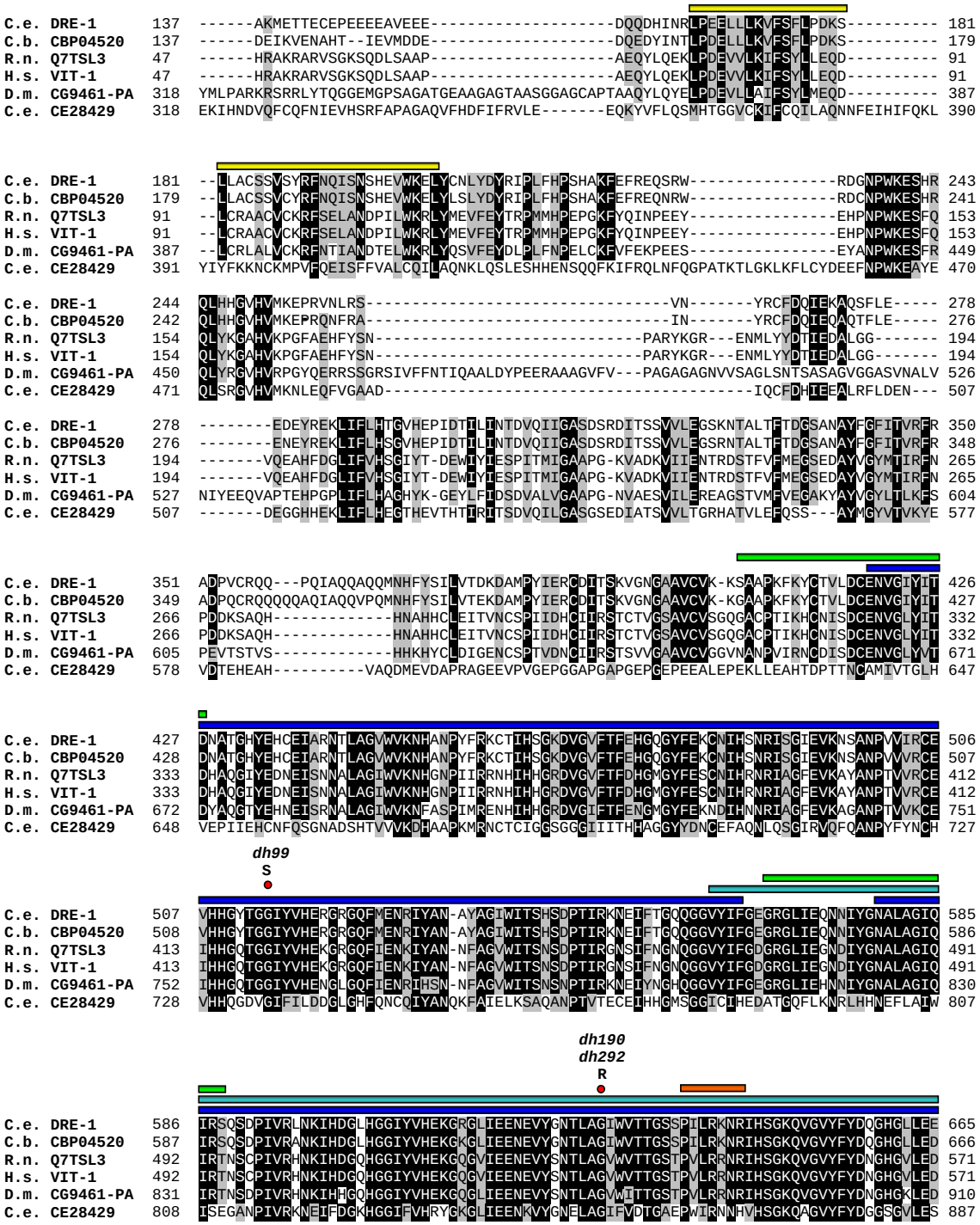

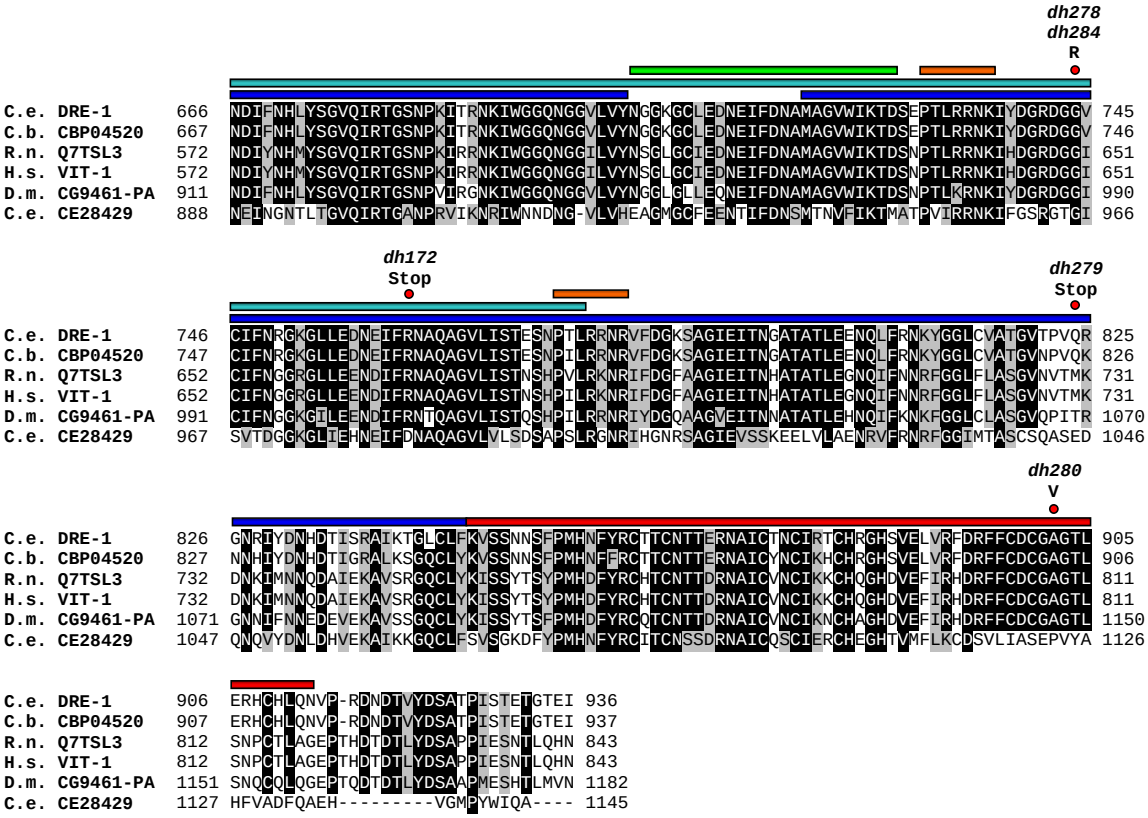

4.7. *dre-1* molecular lesions

Sequence analysis of *dre-1* alleles revealed that all mutations were located in the C-terminal half of the protein (Figure 4.5.). Moreover, many mutations clustered in the CASH/PbH1 domains (6/8). Remarkably, five of these (*dh99, dh190, dh292, dh278, dh284*) affected conserved glycine residues within the parallel beta-sheets, implying that this structure was disrupted. One mutation was found in the NosD domain solely (*dh279*) and one in the Zinc finger (*dh280*) (Figure 4.5., Table 4.2.). Six were missense mutations, while two (*dh172* and *dh279*) were stop codons (Figure 4.5., Table 4.2.), all of which gave similar hypomorphic phenotypes. Because none of the mutations resulted in a molecular null, we searched for a deletion by performing PCR on pooled mutagenized DNA samples. *dre-1(hd60)* deleted 1262 bp removing exons 1-3 and with them the functionally important F-box domain. The deletion started in the promotor region 110bp upstream of the start codon and ended in exon 3, deleting almost half of this exon (Figure 4.5., Table 4.2.). This deletion is strongly predicted to disrupt the entire DRE-1 protein function. Accordingly, phenotypic analysis of *dre-1(hd60)* revealed that the deletion caused more severe embryonic and larval phenotypes (see 4.13.).

4.8. *dre-1* loss-of-function versus gain-of-function mutations

Because most *dre-1* mutations were located in the C-terminal half of the protein, we wondered whether the corresponding mutant defects represented loss or gain of function phenotypes. Consistent with the former, *sDf36/dh99* enhanced the alae gap phenotype of *dh99* from 45% to 82% (Table 4.4). In addition, *dre-1* RNAi fed to wild type gave phenotypes similar to *dh99* including adult alae gaps, precocious seam fusion at the L3 molt and SynMig phenotypes with *daf-12* (Table 4.3., Table 4.4.). Finally, *dre-1* RNAi enhanced both the penetrance and expressivity of *dh99* phenotypes (Table 4.4.). In *dh99* alone, 45% of animals displayed adult alae gaps in 19 % of the cells. In contrast, when *dre-1(dh99)* animals were fed *dre-1* RNAi 95% of animals displayed alae gaps. Oftentimes gaps covered half of the animal (Table 4.4.), and 15% of animals did not contain any adult alae at all. Similarly, *dre-1(dh99)* alone had a weak delayed gonad migration defect, but when fed *dre-1* RNAi, 93% of animals exhibited a strongly delayed Mig phenotype (Table 4.3.). These findings suggest that *dre-1(dh99)* is a reduction-of-function, rather than a gain-of-function mutant.

Table 4.2. *dre-1* molecular lesions

dre-1 alleles	Position in protein (domain)	Location in cosmid K04A8
dh99	G514 → S (CASH)	1835 GGT → AGT
dh190, dh292	G629 → R (CASH)	1490 GGA → AGA
dh278, dh284	G744 → R (PbH1)	952 GGA → AGA
dh172	R762 → Stop (CASH)	898 CGA → TGA
dh279	Q824 → Stop (NosD)	609 CAA → TAA
dh280	A902 → V (Zinc finger)	127 GCT → GTA
hd60	deletion of first 388aa (exon 1 – 3) (F-box)	4065 to 2803
dre-1(RNAi)	between F-box and first PbH1	2957 to 2470

4.9. The *dre-1* 3'UTR lacks *let-7* and *lin-4* binding sites

A common mechanism of temporal regulation of heterochronic activities is that of translational control through miRNAs. miRNAs interfere with translation of the target through imperfect antisense base pairing with complementary sites in the 3'UTR of targets. We examined the 3` UTR of *dre-1* by looking for short regions complementary to *lin-4*, *let-7*, *let-7* paralogs (*mir-48*, *mir-84* and *mir-241*) and *mir-69*. However, the 3'UTR of *dre-1* was relatively short and lacked binding sites for these miRNAs. In conclusion DRE-1 abundance may controlled by other mechanisms.

4.10. The heterochronic gonadal circuit

Heterochronic genes are primarily known for their roles in terminal differentiation of the hypodermis (Ambros, 1989; Ambros and Horvitz, 1984), but also function in the developmental timing of the vulva (Bettinger et al., 1997), dauer larva formation (Liu and Ambros, 1989), male tail formation (Euling et al., 1999) and neuronal rewiring (Hallam and Jin, 1998). With our finding that two heterochronic genes, *dre-1* and *daf-12* controlled the timing of gonad migration (see above), we uncovered part of the gonadal circuit of heterochronic genes. We surmised that further examination of heterochronic mutants for a SynMig phenotypes (Synergistic gonad Migration defect) might reveal parallel functions in the gonadal circuit. Therefore, we analyzed the heterochronic genes *lin-29*, *lin-4*, *lin-41*, *lin-14*, *lin-28*, *let-7*, *lin-42* and *hbl-1* for a SynMig phenotype in *dre-1* or *daf-12* mutants. We either used double mutants or knocked down gene function by RNAi. For evaluation, the different Mig phenotypes have been divided into two major categories (Figure 4.7.).

Category 1 comprises all severe Mig phenotypes with a strong delay in gonadal migration. In category 1A the DTC never reflex and instead continue migration into head and tail on the ventral muscle bands, which is interpreted as a repetition of S2/S3 pathfinding programs. In category 1B, DTC migrate dorsally on schedule, but fail to turn back towards midbody, and instead migrate into head and tail on the dorsal muscle bands. This is interpreted as a hybrid S3/S4 program. In category 1C dorsal and centripetal migration occur very late when the DTC have already reached head and tail regions, interpreted as a delayed expression of the S4 program.

Category 2 comprises weak delayed Mig phenotypes and is interpreted as a failure to express SA programs. In category 2A, the DTC reflex on schedule, but fail to fully migrate

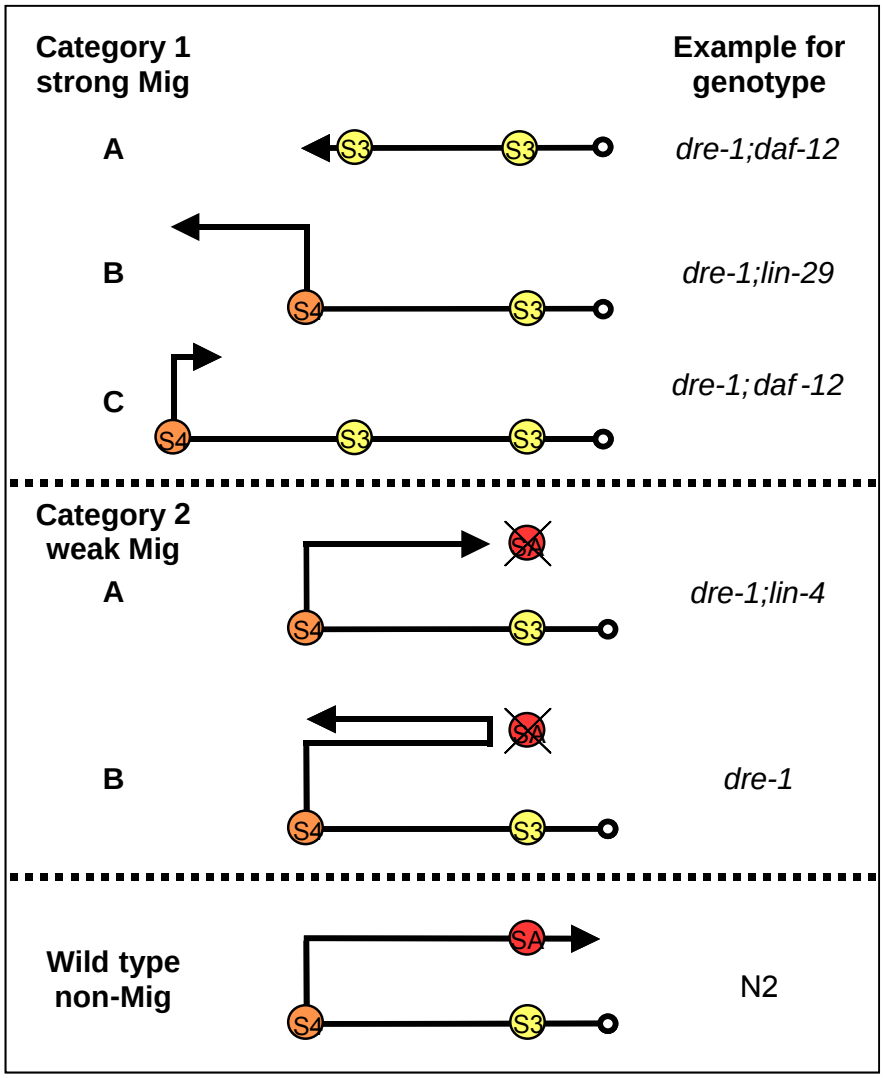

Figure 4.7. Heterochronic gonadal circuit – categories of Mig Phenotypes
For simplification a cartoon of only one gonadal arm is depicted for each category and for wild type. Category 1 comprises variable strong delayed Mig phenotypes; category 2 contains weak migration delays; wild type with wild type gonad. Gonad migration programs are indicated by circles and are color coded. Examples of Mig mutants are indicated on the right side of the cartoon.

back towards midbody. In category 2B, the DTC turn on schedule, but then instead of completing the migration back towards midbody, the arms undergo an extra turn and reverse direction. As described above *dre-1(dh99)*;*daf-12(rh61rh411)* double mutants displayed a strong and penetrant SynMig phenotype that corresponded to category 1A and 1C. (Figure 4.7., Table 4.3.).

The transcription factor *lin-29* is the most downstream gene in the heterochronic seam cell circuit, and displays delayed phenotypes. It is expressed in both gonadal and extragonadal tissues. In the somatic gonad of mutants, the pi uterine cells of hermaphrodites fail to differentiate properly (Newman et al., 2000), and males exhibit a migration defect in

the linker cell (A. Rougvie, personal communication). Interestingly, we found that hermaphrodites doubly depleted of *lin-29* and *dre-1* or *daf-12* exhibited a strong and penetrant defect in DTC migration (Figure 4.7.). In both double mutants a large fraction displayed a strong category 1B Mig phenotype (Table 4.3.). In addition, *lin-29* was picked up in a F2 mutant screen for enhancement of the *dre-1* Mig phenotype (data not shown), revealing that *lin-29* is a potent regulator of temporal programming of the DTC.

The microRNA *lin-4* is a key player within the early timer of the heterochronic seam cell circuit. It is a delayed mutant, reiterating S1 programs. Notably, double mutants of *lin-4* and *dre-1* or *daf-12* were weakly delayed in gonad migration as in category 2A (Figure 4.7.). While less than half of the *daf-12;lin-4* mutants were Mig, 100% of *dre-1;lin-4* displayed the phenotype (Table 4.3.).

The RBBC-RING finger *lin-41* is a precocious mutant and acts in the late timer in the seam cell circuit. It is expressed in gonadal and extragonadal tissues. *lin-41(n2914)* mutants on *daf-12* RNAi resulted in a mainly weak Mig phenotype. 42% of the double mutants belonged to category 2 weak Migs. However, 16% were strong Migs (Table 4.3.). Moreover, *daf-12* mutants on *lin-41* RNAi resulted in a fair fraction of animals with a strong 1B Mig phenotype.

Finally, the Mig phenotype of the nuclear protein *lin-14* (10% category 1), a precocious mutant that acts within the early timer of the seam cell circuit, was enhanced on *daf-12* RNAi. 40% of animals showed a weak category 2 Mig, 8% a strong category 1 delay. *dre-1;lin-14* double mutants were also weakly delayed in gonad migration with a penetrance of 23% (Table 4.3.).

In other heterochronic genes such as the cold shock/Zn finger *lin-28*, the microRNA *let-7* and hunchback *hbl-1* gonad migration was not impaired. Single or double mutants with *dre-1* or *daf-12* were unaffected.

The PAS domain protein LIN-42 is the ortholog of circadian rhythm protein Period of *D. melanogaster*. In *C. elegans* the precocious mutant *lin-42* is thought to act at multiple stages in seam cell development. A particular interesting observation was made analyzing the *lin-42* SynMig phenotypes. *lin-42* alone and double depletion with *dre-1* or *daf-12* were essentially nonMig (Table 4.3.). As shown before, *dre-1;daf-12* double mutants displayed a strong and penetrant SynMig phenotype. Surprisingly, this SynMig was suppressed by the *lin-42* mutation. Triple mutants of *lin-42;daf-12;dre-1(RNAi)* resulted in only 10% of category 1 strong Mig phenotypes (2.5% category 1A, 5% category 1B, 2.5% category 1C) and 2.5% of category 2 weak Mig phenotypes.

Table 4.3. Heterochronic gonadal circuit

Genotype	Single mutant (OP50)	*daf-12* (RNAi)	*daf-12(rh61rh411)*	*dre-1* (RNAi)	*dre-1(dh99)*
N2	0	nd	na	8[d]	na
daf-12(rh61rh411)	1[b]	nd	na	Mig	100 (44[a], 52[c], 4[d])
dre-1(dh99)	10[d]	Mig	100 (44[a], 52[c], 4[d])	98 (79[a], 5[b], 9[c], 5[d])	na
dre-1(dh190)	24[d]	Mig	100 (56[a],18[b], 26[c])	nd	na
lin-29(n546)	0	Mig	96 (2[a], 58[b], 28[c], 8[d])	Mig	100 (28[a], 32[b], 40[c])
lin-4(e912)	0	Mig	42 (2[a], 40[d])	Mig	100[d]
lin-41(n2914)	0	58 (8[a],5[b], 3[c], 42[d])	nd	nd	nd
lin-41(RNAi)	nd	nd	Mig	nd	Mig
lin-14(ma135)	10 (2[b], 8[c])	40 (8[a],32[d])	nd	nd	23[d]
lin-28(n719)	3[d]	5[d]	nd	nd	nd
let-7(n2853ts)[f]	0	nd	nd	nd	0[g]
lin-42(n1089)	0	8[d]	0	nd	0
lin-42(n1089); daf-12(rh61rh411)	0	nd	na	12.5 (2.5[a], 5[b], 2.5[c], 2.5[d])	nd
hbl-1(RNAi)	0	nd	10 (2[b], 8[d])	nd	12[d]

na: not applicable; nd: not determined; n=20-25 adult animals; animals grown at 20°C unless indicated; Mig: Gonadal Migration defect; numbers are percentages of the indicated Mig phenotypes scored by DIC; 0= wild type, animals are nonMig; Mig with no indicated numbers where scored by dissecting microscope only; [a]Mig phenotype of class 1a; [b]Mig phenotype of class 1b; [c]Mig phenotype of class 1c; [d]Mig phenotype of class 2; [f]grown at 25°C; [g]does not enhance *dre-1(dh99)* Mig phenotype at 25°C (1% class 1b; 9% class 2).

In summary, we identified four main players that regulate the timing of gonad migration: *dre-1*, *daf-12*, *lin-29 and lin-4*. *dre-1;daf-12* double mutants exhibited a strong category 1A Mig phenotype, which is interpreted as a repetition of S2/S3 gonad migration programs (Figure 4.7.). Therefore DRE-1 and DAF-12 functions are necessary for S3/S4 program execution. *lin-29;dre-1* or *lin-29;daf-12* double mutants exhibited a category 1B Mig, interpreted as an erroneous S4 program expression. This implies that LIN-29 function is needed for proper S4 program execution. *lin-4* displayed weakly delayed category 2 Mig phenotypes in *dre-1* or *daf-12* double mutants. As this is interpreted as a failure in SA program execution, the presumed function of *lin-4* is the activation of these adult programs. As *lin-42* suppressed the strong *dre-1;daf-12* Mig phenotype it acts downstream by epistasis definition in the timing of gonad migration.

4.11. Heterochronic seam cell circuit

4.11.1. *dre-1* acts upstream of *lin-29*

We showed that *dre-1* was a precocious heterochronic gene that expressed the adult program including seam cell fusion and adult alae synthesis, one stage early at the L3 molt. In order to place *dre-1* in the heterochronic seam cell pathway, we performed genetic epistasis and synergy experiments with known heterochronic mutants. Since precocious adult alae formed by *dre-1* mutants were indistinct, we mainly used precocious seam cell fusion as an indicator for precocious terminal differentiation of the hypodermis.

Genetic epistasis experiments with heterochronic mutants are performed with double mutants of the opposite phenotype i.e. precocious/delayed mutants. By convention, the gene whose temporal fate is adopted acts downstream in the pathway. Ideally, the examined mutants should be null. *dre-1* alleles used were hypomorphic and non-null, since null mutants are embryonic lethal, and thus these experiments must be interpreted with caution. As *dre-1* was a precocious mutant we focused on epistasis relationships with delayed heterochronic mutants. We therefore made double mutants with *dre-1(dh99)* and the delayed heterochronic mutants *lin-29*, *lin-4*, *let-7* and *daf-12*.

The transcription factor *lin-29* is the latest acting, downstream heterochronic gene identified. In *lin-29* mutants seam cell development appears normal until L4. At the L4 molt, however, animals fail to express the SA program resulting in a complete lack of adult alae. The delayed phenotype results from the repetition of S4 larval seam cell division programs. Epistasis analysis of *dre-1(dh99); lin-29(n546)* double mutants placed *dre-1* upstream of *lin-29*. Double mutants neither exhibited the *dre-1* specific precocious adult alae nor precocious seam cell fusion at the L3 molt. Instead, double mutants resembled the retarded

lin-29 phenotype. Animals lacked adult alae completely at the L4 molt (Table 4.4.). These data imply that *lin-29* was epistatic to *dre-1.*

We next determined the epistatic relationship between *dre-1* and *lin-4*. The microRNA *lin-4* plays a key role within the early timer of the heterochronic seam cell circuit, inhibiting LIN-14 and LIN-28 postranslationally to advance to S2 and S3 stages. *lin-4* null mutants reiterate S1 programs inappropriately resulting in a delayed phenotype including absence of adult alae at the L4 molt and the vulvaless (Vul) phenotype (Table 4.4.). *dre-1(dh99);lin-4(e912)* double mutants were indistinguishable from *lin-4* single mutants. Precocious seam cell differentiation was not observed at the L3 molt, but instead the retarded *lin-4* seam cell phenotype at the L4 molt (Table 4.4.). In addition, *lin-4*;*dre-1* double mutants exhibited the retarded vulvaless phenotype of *lin-4* at the L4 molt. Together these data suggested that *lin-4* was epistatic to *dre-1*.

The last retarded mutant that we tested for epistasis was the microRNA *let-7* that initializes the late timer. *let-7* downregulates LIN-41 and HBL-1 posttranslationally to advance to the SA stage. *let-7* null mutants have normal seam cell development until L4, where they fail to execute the SA program, and instead repeat S4 seam cell programs that result in lack of clear adult alae at the L4 molt. Seam cell terminal differentiation occurs at an additional fifth molt. Examination of *dre-1;let-7* double mutants revealed precocious seam cell fusion at the L3 molt, indicating that *dre-1* was epistatic to *let-7* for this phenotype (Table 4.4.). However, at the L4 molt, no adult alae or indistinct adult alae were seen, similar to *let-7*. Surprisingly, we found that *let-7* mutants alone exhibited nearly normal seam cell fusion at the L4 molt (86% of animals). This phenotype has not been reported previously and indicates that other functions largely maintain this aspect of the adult program. In double mutants with *dre-1*, all animals displayed nearly complete fusion of the seams, as in wild type. However, on occasion, some seam cells failed to fuse, revealing *let-7*-like phenotypes. Finally, the *let-7* larval lethality due to uterine prolapse was partially suppressed by *dre-1*. Together, these data indicate that *dre-1* was partially epistatic or acts in parallel to *let-7*, and suggest that other regulators must be downstream of *let-7*.

Epistasis analysis of *dre-1(dh99);daf-12(RNAi)* double mutants placed *dre-1* downstream of *daf-12.* At the L3 molt, mutants displayed the *dre-1* specific precocious seam cell fusion and adult alae gaps at the L4 molt. This is consistent with *daf-12* functioning in early and *dre-1* functioning in late larval temporal development of seam cells.

Table 4.4. *dre-1* seam cell phenotypes and genetic epistasis experiments

Genotype	% of animals with adult alae @L3m[a]	% of animals with adult alae (% of animals with alae gaps) @L4m	% of animals with seam cell fusion@L3m[b]
N2	0	100 (0)	0
ajm-1::GFP	0	100	0
dre-1(RNAi)	10	100 (83)	70[c]
dre-1(dh99) on *dre-1(RNAi)*	nd	85 (95)	90[d]
dre-1(dh99) on L4440	nd	nd	80
dre-1(dh99)	15	100 (45)	85
dre-1(dh99) post dauer	nd	100	nd
lin-4(e912); dre-1(dh99)[e]	0	0	0
lin-4(e912)[e]	0	0	0
daf-12(rh61rh411)	0	100	0
daf-12(rh61rh411); dre-1(dh99)	nd	100 (56)	nd
daf-12(RNAi); dre-1(dh99)	nd	nd	58
dre-1(dh99)[f]	nd	nd	63
let-7(n2853)[f]	0	0	0
let-7(n2853); dre-1(dh99)[f]	nd	0	60
lin-29(n546); dre-1(dh99)[g]	0	0	0
lin-29(n546)[g]	0	0	0
dre-1(dh99)/sDf36	nd	82	nd

nd: not determined; n=20; one side of each animal was scored; animals grown @20°C; [a]% of animals with any adult alae; [b]% of animals with any precocious fusion of the seam cells at L3m using the *ajm-1::gfp* marker; [c]14% animals with abnormal seams*, [d]53% animals with abnormal seams*; [e]100% of animals were Vul (Vulvaless); [f]animals grown @25°C; [g]100% of animals were Pvul (Protruding vulva).
*Irregular pattern of seam cell fusion with patchy interruptions or branching that may be due to abnormal seam cell morphology, differentiation, or positioning.

4.11.2. *dre-1* acts in parallel to *lin-41* and *lin-42*

To elucidate the relationships between *dre-1* and other precocious heterochronic genes acting in late larval stages, we performed genetic synergy experiments. In principle, these experiments could reveal activities that act in parallel or within same pathways. If two genes act in parallel, double mutants should display a strong, synergistic phenotype not observed in either single mutant. When acting in the same pathway double mutant phenotypes should not be enhanced, resembling either single mutant phenotype. These interpretations are most informative when null alleles are used. The weak and impenetrant precocious alae phenotype of *dre-1(dh99*) as well as *dre-1(dh99)* on *dre-1* RNAi, gave evidence that redundant functions must exist. Hence, we analyzed double mutants of *dre-1(dh99* or RNAi)

and other heterochronic loci that exhibited seam cell programming defects similar to *dre-1*: normal seam cell development until L3 molt, where precocious SA program execution (seam cell fusion and adult alae expression) occurs. We therefore tested *lin-41*, *lin-42* and *hbl-1*.

lin-41 encodes an RBCC protein that is proposed to be involved in translational regulation of *lin-29*. In null mutants, about half of the animals have precocious alae at the L3 molt. Of these, about one third of the seam cells express the adult fate (Slack et al., 2000). Similarly, we found that *lin-41* RNAi caused 50% of the animals to have precocious alae, and within these animals about 25% of the seams showed this phenotype (Table 4.5). Thus, *lin-41* RNAi nearly recapitulates the null phenotype. Notably, when we fed *lin-41* RNAi to *dre-1(dh99)* we found that precocious phenotypes were dramatically enhanced. All the animals had full length adult alae at the L3 molt. We conclude that DRE-1(+) and LIN-41(+) act in parallel to prevent SA fates.

lin-42 encodes the *C. elegans* ortholog to the circadian rhythm component Period (Per) of insects and mammals. In *C. elegans lin-42* is implicated in seam cell development (Jeon et al., 1999). We found that *lin-42(n1089)* null mutant resulted in 64 % of seam cells expressing wild type-like adult alae at the L3 molt in nearly all animals. *dre-1* mutation gave patches of indistinct adult alae in 15% of animals at the L3 molt. In contrast, *dre-1(dh99);lin-42(n1089)* double mutants exhibited precocious full length alae in all animals at the L3 molt (Table 4.5.), an enhanced phenotype not observed in either single mutant (Table 4.5.). Moreover, the alae quality improved to that of wild type in double mutants. This synergy showed that DRE-1(+) and LIN-42(+) act in parallel within the heterochronic seam cell circuit to prevent precocious expression of SA fates.

hbl-1 encodes the *C. elegans* homologue of fly Hunchback. Depletion of *hbl-1* by RNAi results in penetrant precocious adult alae phenotypes at the L3m (Abrahante et al., 2003; Lin et al., 2003). We found that *hbl-1* RNAi gave rise to precocious wild type-like adult alae in nearly all animals in which 75% of the seam cells expressed alae. Similarly, depletion of *hbl-1* in the *dre-1* mutant background resulted in a *hbl-1*-like phenotype. This may suggest that *dre-1* and *hbl-1* act in the same pathway. However, since the *hbl-1* precocious phenotype was already very penetrant, this synergy experiment was not conclusive. Further synergy experiments in different mutant backgrounds (e.g. *lin-4, let-7*) should help to resolve this question.

Table 4.5. Genetic synergy experiments of *dre-1*

Genotype	% of animals expressing alae @L3m (% of seam cells expressing adult alae @L3m[a])	% of animals expressing alae @L4m (% of seam cells expressing adult alae @L4m[a])	% of animals exhibiting fusion @L3m (% of Seam cells exhibiting fusion @L3m[b])
N2	0 (0)	100 (100)	0 (0)
ajm-1::gfp	0 (0)	100 (100)	0 (0)
dre-1(RNAi)	10	100 (83)	70%[c] (54)
dre-1(dh99)	15 (33)	100 (81)	85 (52)
lin-41(RNAi)	50 (25)	(100)	nd
lin-41(RNAi);dre-1(dh99)	100 (100)	(100)	nd
lin-42(n1089);dre-1(dh99)	100 (100)	nd	100 (100)
lin-42(n1089)	95 (64)	nd	95 (64)
hbl-1(RNAi)	81 (75)	nd	nd
hbl-1(RNAi);dre-1(dh99)	100 (61)	nd	100 (74)

nd: not determined; na: not applicable; n=10-20; one side of each animal was scored; animals grown @20°C; average number of seams cells that are fused or secreted precocious alae are given; for adult alae and seam cell fusion only V1 to V6 were scored; [a]for scoring adult alae single and double mutants without *ajm-1::*GFP were used; [b]for scoring seam cell fusion single and double mutants in the *ajm-1::gfp* background were used; [c]14% animals with abnormal seams (Irregular pattern of seam cell fusion with patchy interruptions that may be due to abnormal seam cell morphology or differentiation).

4.12. *dre-1* affects molting

C. elegans develops from egg to adult through four larval stages that each culminate in molting. The molt cycle is a convenient landmark for chronological age. One cycle comprises synthesis of a new cuticle, and shedding of the old one, and is accompanied by developmental transitions of the animal. Interestingly, RNAi of *dre-1* produced not only heterochronic gonadal (Table 4.3.) and extragonadal (Table 4.5.) phenotypes, but also molting defects. Therefore, *dre-1* affects both developmental and chronological age.

Feeding *dre-1(dh99)* mutants *dre-1* RNAi caused cuticle shedding defects that resulted from cuticular constrictions at various body regions (Figure 4.8.A). Moreover, worms stuck in their old cuticle (Figure 4.8.B). Oftentimes, the old cuticle remained attached to various parts of the body.

To determine whether *dre-1* played a role at a specific stage, we examined *dre-1(dh99)* animals on *dre-1* RNAi for defects and penetrance at all larval molts. At 20°C only 4% of animals displayed a defect at the L2 molt, whereas 18% affected the L3 and 16% the L4 molt (Table 4.6.). Surprisingly, at 25°C, no molt defects were observed at L1 and L2 molts and only 7% at the L3 molt. However, 40% of the animals exhibited a defect at the L4 molt (Table 4.6.).

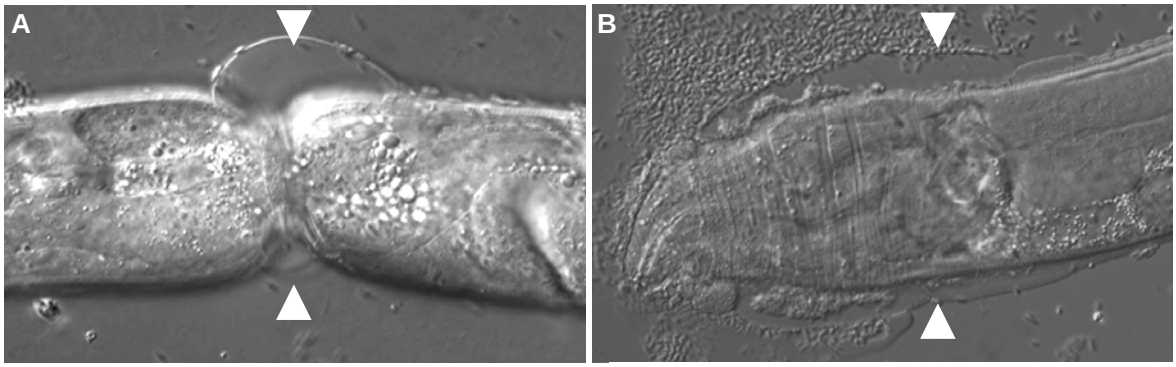

Figure 4.8. *dre-1* molting defects
dre-1(dh99) mutant worms fed *dre-1* RNAi with various cuticle shedding defects. (A) Young adult with cuticular constrictions at mid body. (B) Head of a worm at L3 molt with blisters on cuticle.

Notably, *dre-1* affected all but the L1 molt, with increasing penetrance towards later molts. Furthermore, a delay for various molts was observed with *dre-1(dh99)* animals alone and on *dre-1* RNAi. While *dre-1(dh99)* animals were delayed for the L3 molt only (3.6 h extra; n=7); *dh99* animals on *dre-1* RNAi exhibited a delay in the L1, L2 and L3 molt (Table 4.6. footnotes).

Table 4.6. *dre-1* plays a role in molting

Molt	% of animals with molting defects grown at 20°C[a]	% of animals with molting defects grown at 25°C
egg	1[b]	nd
L1	0	0[d]
L2	4	0[e]
L3	18[c]	7[f]
L4	16	40

nd: not determined; *dre-1(dh99)* fed *dre-1* RNAi. Age was estimated by size by dissecting microscope unless indicated; molting defects were observed by DIC; worms were grown on *dre-1* RNAi for 2 generation prior to experiment; [a]n ≥ 23 for worms; [b]n=210; 3 eggs unhatched, stage unkown; [c]worms were observed by DIC for age for no prior molting defect; [d]worms were little delayed for molt compared to controls; [e]33% delayed for L2m, controls *(dre-1(dh99)* on L4440 not delayed); [f]*dre-1(dh99)* and control animals were delayed for L3m.

Besides molting defects, *dre-1(dh99)* animals on *dre-1* RNAi displayed other phenotypes. Larval lethality was quite frequent (Table 4.7.). Moreover, a particularly prominent phenotype was rupture of uterine/seam junction and/or the rectum (Table 4.7.). In addition, a fraction of young adults had a protruding vulva (Pvul) or an egg laying defect (Egl), where the progeny hatched internally (Table 4.7. footnotes). Animals were also dumpy (Dpy), a phenotype that contrasts sharply with *dh99* mutants, which are long (Lon).

Table 4.7. *dre-1* RNAi yields variable phenotypes

Stage	Sick larvae (%)[a]	Rup (eversions at body cavities) (%)[b]	Lethality (%)[b]
L1	13	0	0
L2	7	0	13
L3	0	20	20
L4	16[f]	40	7
Adult	na	53	7[c]

dre-1(dh99) fed *dre-1* RNAi. n=15-23 animals; age was estimated by size by dissecting microscope; animals were grown on *dre-1* RNAi for 2 generation prior to experiment; Rup: eversions at body cavities result from rupture of uterine/seam junction and/or the rectum; [a]animals grown at 20°C; [b]animals grown at 25°C, [c]egg laying defective, progeny hatches internally; at 20°C 16% and 2% with protruding vulva

4.13. *dre-1* deletion results in embryonic lethality

The *dre-1* deletion *hd60* (Table 4.2.) gave rise to embryonic lethality and early larval arrest. The majority of embryos (98%) developed to the embryonic three-fold stage (n=95, Figure 4.9.) while the age of a small fraction (2%) of embryos could not be determined due to advanced degradation. To see if maternal product could provide residual activity, we subjected the balanced *dre-1* deletion strain to *dre-1* RNAi by feeding. Notably, no additional phenotype was observed, suggesting that arrest at the three fold stage represents the terminal phenotype. Despite arrest, embryos moved vigorously inside their eggshell, indicating they had a hatching problem.

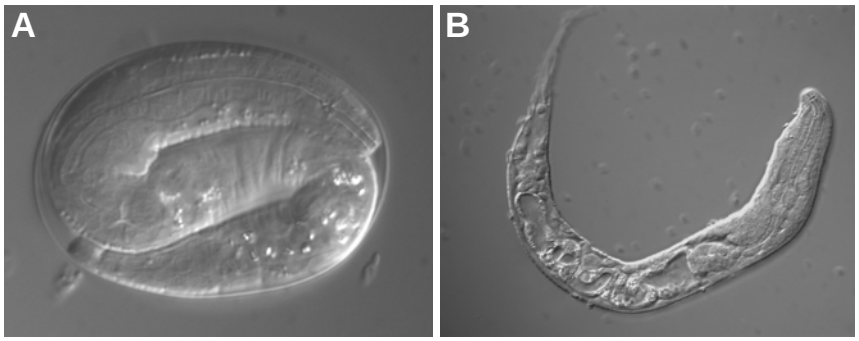

Figure 4.9. *dre-1(hd-60)* deletion results in embryonic lethality and early larval arrest.
dre-1(hd-60) deletion worms. (A) Embryo at the 3-fold stage; (B) Developmentally arrested L1 larva.

A small proportion of embryos hatched. These larvae or larvae freed from their eggshell mechanically, proceeded with development to the L1 or L2 stage. As arrested larvae, they lived up to seven days. Growth arrest presumably resulted from pleiotropic abnormalities. Hatched larvae exhibited uncoordinated movement (Unc) as they moved slowly and in a non-sinusoidal manner. Moreover, they had a swollen gut with accumulation of superficial

granules and were constipated. In addition, some head neuronal cells were often swollen as after stress exposure. Some larvae also had a smaller body size (Sma).

4.14. Expression pattern

To investigate *dre-1* expression, we used the 4,0 kb promotor, the full length 3,9 kb *dre-1* genomic region as well as 0.924 kb downstream of the stop codon (including the 336 bp long 3' untranslated region) and inserted *gfp* in-frame close to exon 1 (Figure 4.10. middle panel). Analysis of different extrachromosomal arrays (*dhEx346, dhEx376*) and an integrated line (*dhIs378)* confirmed the expression pattern. *dre-1* was expressed most prominently in neurons, including neurons in head, tail, ventral cord as well as peripheral neurons. Expression was strong in the excretory cells, muscle cells of the body wall, vulva, anal depressor muscle, the procorpus, the most posterior cells of the metacarpus, and the pharyngeal/intestine junction. In the epidermis, expression was seen in vulval cells and their precursors, and weakly in seam cells, and perhaps head and tail hypodermal cells (Figure 4.10.C). Main body hypodermis (hyp7) expression was absent. Finally, expression was seen in a handful of somatic gonadal cells and the Distal Tip Cells (Figure 4.10.B). *dre-1* was expressed more prominently in the nucleus and reduced in the cytoplasm. Expression was detected from embryo to adult but relative levels of expression by stage were not determined because of mosaicism of the arrays.

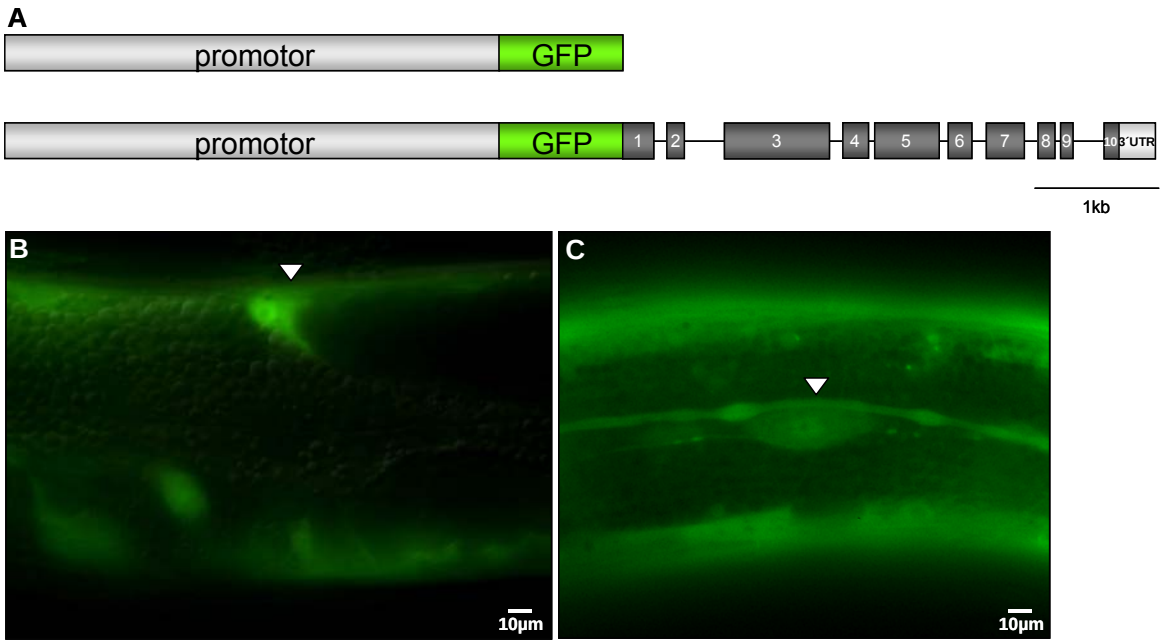

Figure 4.10. *dre-1* expression
(A) *dre-1promotor::gfp* construct and *dre-1::gfp* construct. Promotor and 3'UTR in light grey, *gfp* in green, exons in dark grey.
(B) and (C) L4 worm. *dre-1::gfp* is expressed in the cytoplasm and nucleus of (B) Distal Tip Cell (arrowhead), and (C) in seam cells (arrowhead).

Similar results were obtained with the *dre-1* promotor construct. For this construct we used a 4,0 kb promoter region and fused it to *gfp* (Figure 4.10.A). In contrast to the contstruct containing the *dre-1* ORF, the *dre-1promotor::gfp* was expressed in the nucleus and cytoplasm at similar levels.

4.15. *dre-1::gfp* partially rescues the *dre-1* deletion

To examine the *dre-1::gfp* construct for function, we tested if it could rescue the *dre-1* deletion phenotype. As described earlier, *dre-1* deletion animals arrested development at the embryonic three-fold stage or died as young larvae. Strikingly, 57% of the deletion animals carrying the *dre-1::gfp Ex346* array progressed to reproductive adults (Table 4.8.). This partial rescue proved the *dre-1::gfp* construct to be functional. Interestingly, it also produced intermediate mutant phenotypes observed with *dre-1* alleles as well as with *dre-1* RNAi. Among them were molting defects, larval lethality and eversions at body cavities at nearly all larval stages (Table 4.8.). In addition, heterochronic phenotypes such as the gonadal migration (Mig) defect and the alae gap seam cell phenotype were detected (Table 4.8.). A particular interesting result came from the analysis of molting defects. 13% of the animals exhibited a molting defect at the L1 molt, a phenotype not observed with *dre-1* RNAi.

Table 4.8. *dre-1::gfp* partially rescues *dre-1* deletion

Stage	Sick larvae	Molt	Degraded	Rup	Mig	wt
Egg	na	8[a]	na	na	na	92
L1[b]	8	13	31	0	na	61
L2[c]	10	0	35	6	na	42
L3[d]	nd	0	55	0	0	45
L4	nd	43	6	0	3	91
Adult	nd	na	0	0	6	57

na: not applicable; nd: not determined; animals with mutant phenotypes displayed weak to strong GFP expression; some animals displayed several mutant phenotypes; n=30 animals unless indicated; Rup: eversions at body cavities result from rupture of uterine/seam junction; [a]3 fold egg, unable to hatch; [b]2 animals with extra tissue @ head region, n = 13; [c]2 animals with extra tissue @ head region; [d]n=11

4.16. Aging experiments

daf-12 mutants affect the longevity of *C. elegans* in various ways. For example, *daf-12* null mutants mildly suppress the longevity of weak *daf-2*/insulin-like receptor mutants, but enhance the longevity of strong alleles (Gems et al., 1998). We asked whether *dre-1* influences life span as well. *dre-1* alone had a slightly increased mean and maximum life span compared to wild type (Figure 4.11., Table 4.9.). In addition, it slightly reduced the mean life span of the weak allele *daf-2(e1368)* and increased the mean and maximum life

spans of strong allele *daf-2(e1370)* (Figure 4.11., Table 4.9.). Thus, *dre-1* influenced *daf-2* longevity in a manner similar to *daf-12.* However, *daf-12* extends *daf-2* longevity to a greater extent.

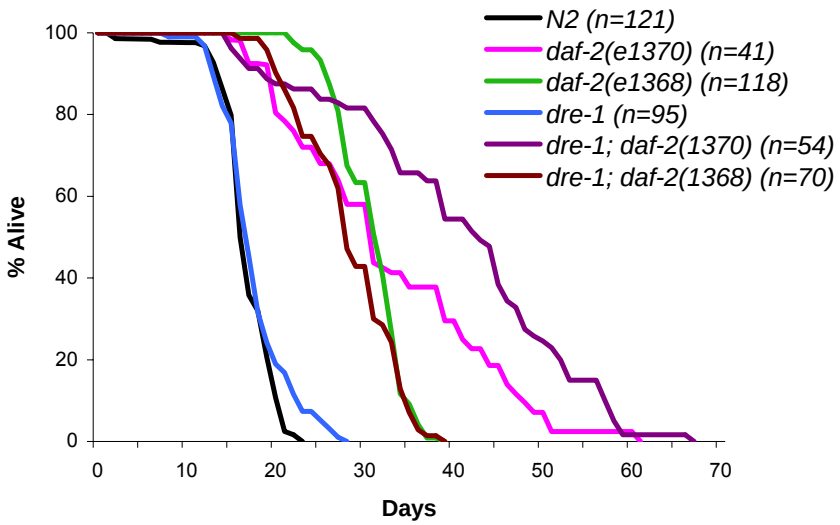

Figure 4.11. Aging graph of *dre-1.*

Table 4.9. Life spans

Genotype	Mean life span (d)	Maximum life span (d)
N2	17	23
daf-2(e1368)	31	39
daf-2(e1370)	31	62
dre-1(dh99)	18	28
dre-1(dh99);daf-2(e1368)	28	39
dre-1(dh99);daf-2(e1370)	39	67

4.17. DRE-1 complex

F-box proteins are characterized components of SCF (Skp1, Cullin, F-box) E3 ligase complexes. The molecular identity of *dre-1* as a F-Box protein, containing a zinc finger in N-recognin, suggests that it may be a component of a SCF complex. To test this hypothesis, we screened for potential members of this complex, *C. elegans* Skp1 and Cullin homologues, for *dre-1* like phenotypes by RNAi. First, we screened for a SynMig phenotype in the *daf-12* mutant background, and second for an enhancement of *dre-1* phenotypes in the *dre-1* mutant background (enhancement of Mig and molting defects) (Table 4.10.). Specifically RNAi of *skr-1*, a yeast Skp1 homolog and *cul-1*, a cullin, yielded strong synergistic Mig phenotypes in the *daf-12* mutant (Table 4.10.). Moreover, they enhanced the

Table 4.10. RNAi screen for putative SCF components of DRE-1 complex

dsRNA construct	N2 reported phenotypes (detected phenotypes)	*daf-12(rh61rh411)* animals with Mig phenotype, (other phenotypes)	*dre-1(dh99)* animals with Mig and Molt phenotypes, (other phenotypes)
L4440	wt	0	+
dre-1(dh99)	**+** (Rup)	**+++**	**+++, Mlt**
skr-1	Emb **+** (Emb, Rup, Clr)	**+++**, (Lon, Pvl, Rup, Emb)	**+++, Mlt** (Unc, Lon, Egl)
skr-2	Emb, Gro, Pvl, Unc	0	0
skr-3	wt	+	0
skr-5	wt	+/++	0
skr-6	wt	+	0
skr-8	Emb, Bmd, Ste	0	0 (Lon)
skr-9	Emb, Ste, Lva	+	0
skr-11	wt	0	+ (Clr)
skr-12	wt	++ (Bmd, Lon)	0
skr-13	wt, Ste	0	++
skr-15	wt	0	0
skr-17	wt, Emb	0	0
skr-18	Unc, Rup, Pvl, Gro	++	0
skr-19	wt	+	0
skr-20	wt	++	+
skp-1 component C16D2.1	wt	+/++	0
skp-1 component F18A11.5	wt	0	0
elc-2	Emb, Lva	0	0
cul-1	**+** (Lon, Emb, Clr)	**+++** (Lon, Emb, Rup)	**+/+++ Mlt** (Emb, Lon, Rup)
cul-4	Gro Pvl Rup Stp, Unc	+ (Lva)	+
cul-5	wt	+	0
cul-6	wt	+	+ (Lon, Lva)
apc-1	Mei, Ste	+	+ (Lon)
rbx-1	+ (Emb, Lon)	+ (Emb, Rup)	0 (Emb, Lon)

dsRNA construct	N2 reported phenotypes (detected phenotypes)	*daf-12(rh61rh411)* animals with Mig phenotype, (other phenotypes)	*dre-1(dh99)* animals with Mig and Molt phenotypes, (other phenotypes)
ubc-3	0	0	0
C05C6.8	0	0	0

Experiments were repeated once; animals grown at 20°C, n ≥ 20 RNAi was performed by feeding bacteria expressing target dsRNA; young adults were scored by dissecting microscope; 0: no Mig phenotype; (+): weak delay in gonad migration detected as white patches on the dorsal side of the animal/Mig blibs; (++) and (+++): strong delay in gonad migration detected as a white stripe on the dorsal side of the animal whereby (++) indicates that less than 50% of animals are strong Mig and (+++) indicates that more than 50% of animals are strong Mig. Emb: Embryonic lethal; Lon: Animals with an extended body length; Pvul; Protruding vulva; Rup: Ruptered, eversions at body cavities; Unc: Uncoordinated movement; Egl: Egg-laying defective; Bmd: Body morphology defect; Ste: Sterile; Lva: Larval arrest; Clr: Clear appearance; Stp: Sterile progeny; Mei: Defective meiosis.

Mig and molting phenotypes of *dre-1(dh99)* (Table 4.10.). Furthermore, knock down of *skr-1* and *cul-1* resembled *dre-1* in its weakly delayed gonad migration and the epidermal alae gap phenotypes (Table 4.11.). However, precocious seam cell fusion needs to be analyzed. These genetic data suggest that DRE-1 might function in an SCF E3-ligase complex containing CUL-1 and SKR-1.

We also tested other potential components of SCF complexes as the Ring finger *rbx-1* as well as *ubc-3*, the E2 ubiquitin conjugating enzyme, involved in the transfer of ubiquitin onto the target protein, by RNAi using same experimental set ups as described above. However, neither *rbx-1* nor *ubc-3* led to *dre-1* like phenotypes.

To confirm genetic data we are currently testing for *in vitro* and *in vivo* interactions of SKR-1 and CUL-1 and will additionally test for further putative components of the DRE-1 SCF complex by RNAi.

Table 4.11. RNAi experiments with candidates of DRE-1 complex

dsRNA construct	% of N2 animals with weak delay in gonad migration (Mig phenotype)	% of N2 animals with alae gap phenotype
L4440	0	0
dre-1	8	60
skr-1	15	50
cul-1	13	75

Animals grown at 20°C, n = 20, RNAi was performed by feeding bacteria expressing target dsRNA; young adults were scored by DIC; 0: no Mig or alae gap phenotype.

In protein interaction studies of *C. elegans* the predicted BTB protein C05C6.8 was found to interact with DRE-1 (Li et al, 2004). BTB proteins have been identified as components of E3 ligase complexes. We genetically tested this BTB protein by RNAi screening for SynMig phenotypes in the *daf-12* and enhancement of *dre-1* phenotypes in the *dre-1* mutant background. Depletion of C05C6.8 did not show *dre-1* like gonadal Mig phenotypes

suggesting that C05C6.8 may not function with DRE-1 in gonad development (Table 4.10.). If it functions with DRE-1 in seam cell development awaits further analysis.

Part II – *dre-2*

4.18. *dre-2* is delayed in gonad migration

The *dre-2(dh184);daf-12(rh61rh411)* double mutant was strongly delayed in gonad migration (Figure 4.12.D, Table 4.13.). Interestingly, among the 63% of the animals exhibiting a SynMig phenotype, two different Mig phenotypes could be distinguished: 43% displayed a category 1A *daf12(rh61)*-like Mig phenotype. DTC failed to reflex and instead continued to migrate into head and tail, which is interpreted as a repetition of S2/S3 pathfinding programs. The remaining 20% exhibited a category 1B Mig: At mid-L3 the DTC halted, reoriented and moved dorsally across the lateral hypodermis on schedule, but then failed in the second reorientation phase. Instead of moving centripetally, DTC migrated into head and tail. *dre-2* alone was also strongly delayed in gonad migration, exhibiting a category 1B Mig with a penetrance of 25% (Table 4.13.). Occasionally, *dre-2* exhibited a weak delayed gonadal cell migration defect such as mispositioned gonadal arms that failed to complete migration towards midbody (Figure 4.12E).

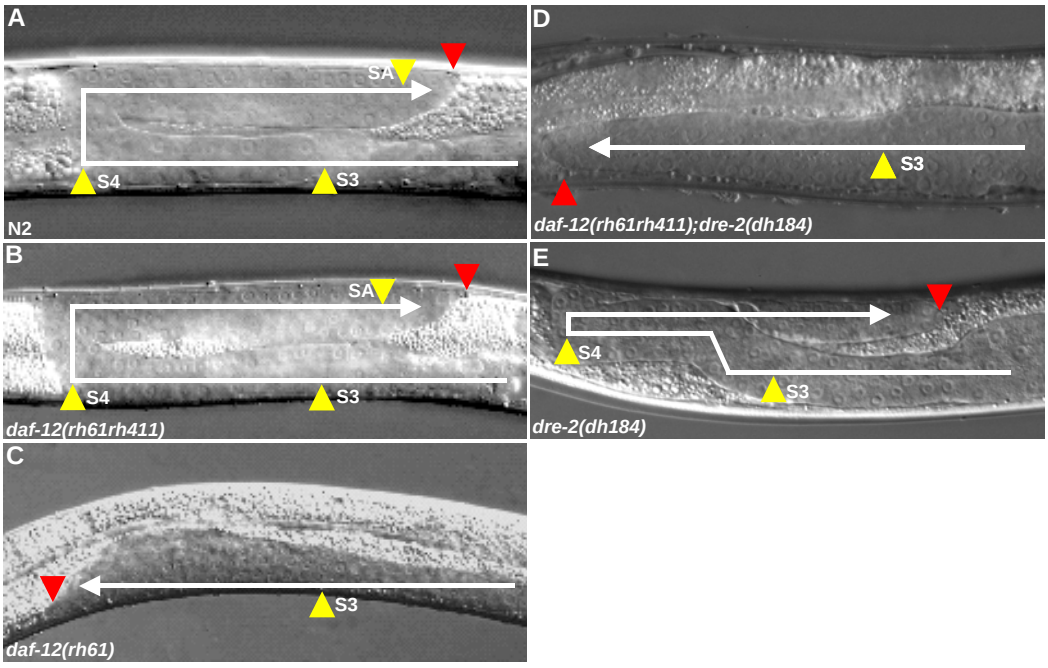

Figure 4.12. Gonadal heterochrony.
Gonadal Mig phenotypes of *daf-12* and *dre-2* single and double mutants. (A) wild type N2 (B) *daf-12* null mutant *rh61rh411* (C) *daf-12* gain-of-function mutant *rh61* (D) *daf-12(rh61rh411);dre-2(dh184)* double mutant (E) *dre-2(dh184)* single mutant. White lines show migration of the gonad. Red arrowhead indicates distal tip cell; yellow arrowheads the starts of appropriate stage-specific gonadal migration programs (S3, S4, SA).

The synergistic Mig phenotypes seen in *daf-12(rh61rh411)*;*dre-2* double mutants suggest that *daf-12* and *dre-2* could act in parallel to promote S3/S4 programs in the gonad. At least *daf-12*, as a nuclear hormone receptor, could do so on a transcriptional level (Antebi et al., 1998).

Table 4.13. *dre-2* enhances *daf-12 (rh61rh411)* delayed phenotypes

Genotype	% strong Mig	% Adult alae gap
dre-2(dh184)	25	0
dre-2(dh184); daf-12(rh61rh411)	63	25

n=25 animals; worms grown at 20°C.

4.19. Seam cell heterochrony - *dre-2* may be a delayed mutant

daf-12 mutants are retarded in development. The *daf-12* mutant *rh61*, which contains a mutation in the ligand binding domain, exhibits an alae gap phenotype, where seam cells fail to execute the adult program. These late defects result from programming errors of previous stages. *daf-12* null mutants repeat S2 seam cell programs in L3 occasionally, but express the adult program on schedule at the L4 molt. *dre-2* alone had no seam cell phenotype. Surprisingly, double depletion of *dre-2* and *daf-12* resulted in an adult alae gap phenotype (Table 4.13.). This may indicate that *dre-2* might have enhanced the heterochronic delayed seam cell phenotype of *daf-12* null.

Interestingly, *dre-2* suppressed the precocious alae phenotype of *lin-42*. Alone 100% of the *lin-42(n1089)* mutant animals had precocious adult alae at the L3 molt. In contrast, only 11% of *dre-2;lin-42* double mutants exhibited the phenotype (Table 4.14).

In conclusion, *dre-2* may be a delayed heterochronic mutant due to the fact that it enhances *daf-12* delayed phenotypes, and conversely suppresses *lin-42* precocious phenotypes.

Table 4.14. *dre-2* suppresses *lin-42(n1089)* precocious alae phenotype

Genotype	% of worms with Adult alae @L3m
dre-2(dh184)	0
lin-42(n1089)	100
dre-2(dh184);lin-42(n1089)	11

n=20 animals; worms grown at 20°C.

4.20. *dre-2* exhibits pleiotropic defects

dre-2 mutants exhibitied several other phenotypes (Table 4.15.). At 20°C, 26.5% of animals were embryonic lethals; 16% arrested development at different larval stages (L1 to L4). Notably, only 57.5% progressed development to reproductive adult. Moreover, 2.5% of adults displayed ruptured uterine/seam cell junction (Rup) and some animals had a smaller body size (Sma). The larval arrest and subsequent lethality presumably resulted from variable body morphology defects (Bmd) and differentiation problems. Misshapen larvae were often uncoordinated (Unc) in movement or paralyzed. In addition, some larvae exhibited a swollen gut.

Table 4.15. *dre-2(dh184)* pleiotropic phenotypes

phenotypes	% of worms with phenotype
embryonic arrest	26.5
larval arrest (L1-L4)	16
Rup	2.5
reproductive adult	57.5

n= 572; animals grown @ 20°C; Rup: Rupture, evertions at body cavities resulted from rupture of uterine/seam junction.

4.21. Mapping *dre-2*

Snip mapping placed *dre-2* to the very left arm of chromosome I. Using dense snip markers, *dre-2* was mapped between the snipSNP markers pKP1102 (-15.24) and pKP1016 (-12.10), roughly between the genes *spe-15* and *rpa-1* (Figure 4.13.). Candidates that mapped to the determined region were tested using RNAi to knock down gene function. As *dre-2;daf-12* double mutants displayed a severe Mig defect, we exposed *daf-12(rh61rh411)* worms to RNAi of candidates. None of the tested candidates yielded a strong Mig defect, indicating that the gene of interest was not among them. We are currently using 3 factor mapping to narrow down the region to a smaller interval.

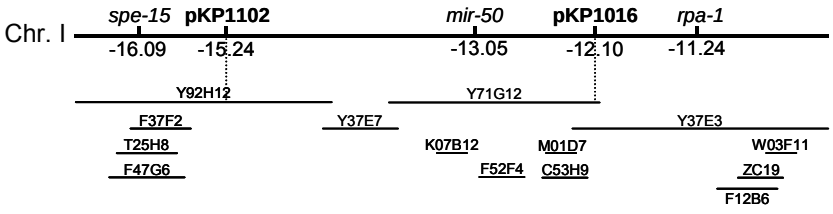

Figure 4.13. *dre-2* genomic organization
dre-2 maps to the very left of linkage group I between the snipSNPs pKP1102 and pKP1016. YACs, cosmids and pKPs are indicated.